



Intra-seasonal and seasonal variability of the Northern Hemisphere extra-tropics

Cristiana Stan¹ · V. Krishnamurthy²

Received: 21 January 2019 / Accepted: 21 May 2019 / Published online: 28 May 2019
© Springer-Verlag GmbH Germany, part of Springer Nature 2019

Abstract

The natural variability of the Northern Hemisphere extra-tropics is studied at seasonal and intra-seasonal time scales. Nonlinear oscillations in the extra-tropics are extracted from daily anomalies of 500-hPa geopotential height for the period 1979–2012 using a data-adaptive method. Three propagating oscillations with broad-band spectra centered at 120, 45, and 28 days are found. When combined, the oscillations explain up to 30% of the natural variability of the extra-tropics on the intra-seasonal to seasonal time scales. These oscillations share some features with the circumglobal wave guide and in some phases of their lifecycles they project onto the canonical teleconnection patterns. When used as predictors in a simple linear regression model with 2-m temperature as predictand, the mid-latitude oscillations extend the potential predictability of dependent variable to about 20 days.

Keywords Mid-latitude atmosphere · Intraseasonal variability · Atmospheric oscillations

1 Introduction

The variability of the climate system as a whole is characterized by a continuous distribution across all frequencies (Hasselmann 1976). However, the skill of predictions beyond the deterministic range (1–2 weeks) has yet to catch up with the forecast skill of weather prediction. Despite the advances made in the development of coupled climate models and their usage by forecasting centers, intra-seasonal to seasonal predictions are still challenging. Apart from modeling concerns, there is a critical need to understand what can be predicted on climate time scale and to identify the sources of long-term predictability. Advancing the prediction capability to sub-seasonal and seasonal time scales and bridging the gap between weather and climate predictions offer potential societal benefits, and the source of predictability at these time scales is the existence of natural modes of variability (National Academy of Science 2016).

While the seasonal variability of most geographical regions is explained by the variations in the solar irradiance upon the earth's surface, a significant fraction of this variability is attributed to internal dynamics of the climate system. The intra-seasonal and seasonal variability of the tropics have been well studied whereas the variability of the Northern Hemisphere's extra-tropics on these time scales is almost an uncharted territory (Stan et al. 2017). The Madden–Julian Oscillation (MJO) in the tropics provides a good example of the usefulness of extracting the near-regular oscillation embedded in the climate variability and to exploit such behavior for extended-range predictability (e.g., Wheeler and Hendon 2004; Gottschalck et al. 2010). The observed connections between the MJO and the Northern Hemisphere (NH) midlatitude variability (Zhang 2013) explain some fraction of the NH variability on intra-seasonal to seasonal time scales. However, the tropical forcing is mostly a modulator of the intrinsic variability of the mid-latitudes. For example, Weickmann and Berry (2009) have shown that the Global Wind Oscillation, which encompasses the MJO and midlatitude process exhibits sub-seasonal variability that cannot be explained by MJO.

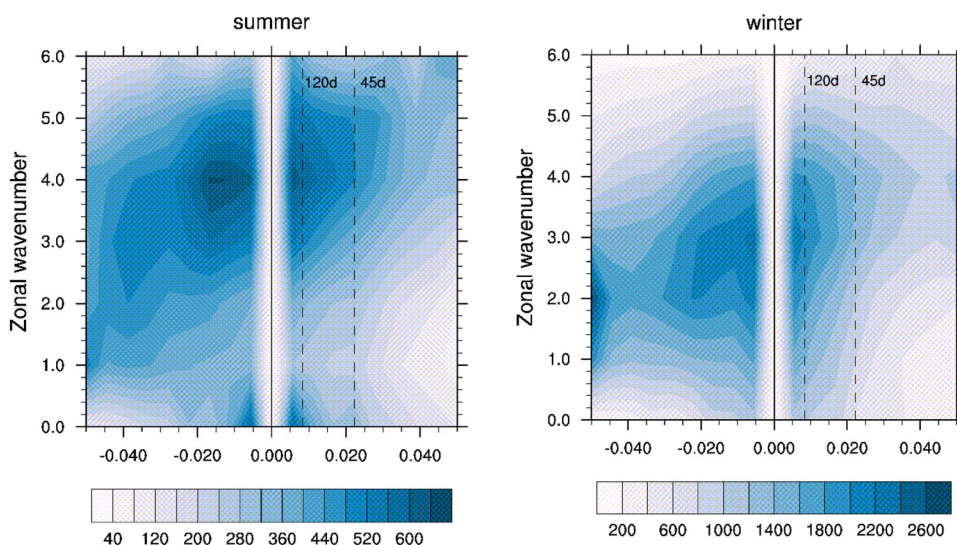
Wave-frequency spectra of midlatitude geopotential height show a concentration of power at intra-seasonal and seasonal timescales during both summer and winter (Fig. 1). The asymmetric amounts of power in the eastward

✉ Cristiana Stan
cstan@gmu.edu

¹ Department of Atmospheric, Oceanic and Earth Sciences, George Mason University, Fairfax, VA 22030, USA

² Center for Ocean-Land-Atmosphere Studies, George Mason University, Fairfax, VA, USA

Fig. 1 Wavenumber-frequency spectra of 500-hPa geopotential height averaged over 30°–75°N. Summer, defined as May–October (left panel) and winter defined as November–April (right panel) were calculated for each year, and then averaged over all years of data (1979–2012). Only the climatological seasonal cycle was removed before the calculation of the spectra. Eastward propagation is represented by positive frequency whereas westward propagation is represented by negative frequency. Units are in $\text{m}^4 \text{s}^{-4}$ per frequency interval per wavenumber interval. The bandwidth is $(180 \text{ day})^{-1}$



and westward direction suggest the existence of propagating oscillatory modes. Previous studies based on empirical analysis suggest that variability of the NH extra-tropics falls into three broad categories of (1) persistent, geographically fixed anomalies, (2) propagating or standing waves (Ghil and Mo 1991; Plaut and Vautard 1994), and (3) circumglobal wave guide patterns (Kushnir 1987; Thompson and Wallace 1998; Branstator 2002; Weickmann and Berry 2007, 2009). The North Atlantic Oscillation (NAO), the Pacific North American (PNA) patterns, and propagating waves in the time range of 20–45 days are examples of regional variability arising from large-scale atmospheric dynamics in the NH extra-tropics.

The waveguide patterns can be confined to the vicinity of the jet streams or described as a zonally symmetric annular mode (e.g., Arctic Oscillation, AO). While there is good observational and modeling evidence that these modes of variability exhibit trends on intra-seasonal to seasonal variability (Thompson and Wallace 2000; Franzke and Feldstein 2005; Kushnir et al. 2006; Gerber et al. 2008; Johnson and Feldstein 2010), the oscillatory characteristics of NH mid-latitudes variability is an open question. For example, some studies show that singular spectrum analysis (SSA) of the NH extra-tropics indicates the presence of global modes of oscillation with periods of about 48 and 23 days (Ghil and Mo 1991), whereas other studies using power spectrum analysis (Wunsch 1999; Feldstein 2000) or empirical mode decomposition (Franzke 2009) of regional patterns find evidence for oscillatory behavior only at longer timescales.

Although the tropical variability is emerging as a potential source of predictability for the NH sub-seasonal to seasonal variability, the role of intrinsic variability of the extra-tropics is also important for these time scales. The existence of oscillatory modes of NH variability on a daily time scale can bridge weather and climate and establish the

basis for extended-range predictability. Applying a data-adaptive method on daily anomalies of geopotential height at 500-hPa over the NH extra-tropics, we establish the existence of at least three nonlinear, propagating oscillations at intra-seasonal to seasonal time scales and demonstrate the potential predictability of these oscillatory modes for 2-m temperature over North America.

The method used to extract the oscillations is described in Sect. 2, while the characteristics of the oscillations are analyzed in Sect. 3. The impact of oscillatory modes on the extended-range predictability is evaluated in Sect. 4. Summary and conclusions are provided in Sect. 5.

2 Data and methods

The data sets used in this study were obtained from the European Centre for Medium-Range Weather Forecasts Reanalysis—Interim, ERA-Interim (Dee et al. 2011). We have used daily means of geopotential height, zonal and meridional velocity components, surface pressure, and surface temperature for the period 1979–2012. These fields are on a horizontal grid with a resolution of approximately 0.703° at various vertical levels. The daily climatology for each calendar day was computed by averaging over the period 1979–2012. The daily anomalies were obtained by subtracting the daily climatology from the daily means for each calendar day. For the multivariate linear regression model, the 2-m temperature from the North American Regional Reanalysis (Mesinger et al. 2006) was used along with the all-season real-time multivariate (RMM) MJO index from the Center for Australian Weather and Climate Research (Wheeler and Hendon 2004). The index is computed using NOAA Interpolated Outgoing Longwave Radiation dataset (Liebmann and Smith 1996) and NCEP/NCAR Reanalysis 1 (Kalnay et al.

1996). Daily teleconnection indices for NAO, AO and PNA were obtained from the National Oceanic and Atmospheric Administration Climate Prediction Center (NOAA/CPC).

To extract the daily modes of variability, we applied the multi-channel singular spectral analysis (MSSA) method (Ghil et al. 2002) on daily anomalies of 500-hPa geopotential height over the domain (0° – 360° ; 30° – 75° N) for all days during the period 1979–2012 using a lag window of 241 days at one-day interval. The MSSA was applied on the data with different lengths of the lag window in a systematic manner. The choice of 241-day lag window assures that the MSSA resolves the periods of all the oscillatory modes reported in this study. The application of the MSSA with different lag windows also confirmed that the results are stable with respect to the choice of the lag window. The MSSA is a data-adaptive method, which decomposes the original time series of spatial maps of total anomalies into space–time patterns of nonlinear oscillations, persistent modes and trends embedded in the climate time series. This method has been successfully applied to study the oscillatory dynamics of weakly nonlinear climate systems (Raynaud et al. 2005), oscillations over the Indian monsoon region (Krishnamurthy and Shukla 2007; Krishnamurthy and Achuthavari 2012), and the coupled dynamics of the ocean–atmosphere system (Feliks et al. 2010, 2016; Vanitsem and Ghil 2017). The MSSA yields eigenmodes with lagged maps of space–time empirical orthogonal functions (ST-EOFs) and space–time principal components (ST-PCs). The eigenmodes are arranged in the descending order of the eigenvalues, which represent the variance explained. The ST-EOFs and ST-PC of each eigenmode are multiplied to obtain the reconstructed component (RC) of the eigenmode (Ghil et al. 2002). Each RC has the same spatial and temporal dimensions as the original time series and correctly captures the phase embedded in the original time series. The sum of all the RCs returns the original time series of spatial maps. An oscillation emerges as a pair of eigenmodes with almost degenerate eigenvalues. The ST-EOFs and ST-PC of the pair are in quadrature. The RCs of the pair are added to obtain the total RC of the oscillation. The phase $\theta(t)$ and amplitude $A(t)$ of the oscillation are determined as a function of time t by the first principal component of the RC of the oscillation (Moron et al. 1998). The space–time structure of the extracted oscillation is studied through phase composites of RC or any other field. For this purpose, the phase, which varies from 0 to 2π for each cycle, is divided into eight equal intervals each of length $\pi/4$. The phase intervals span $(k-1)\pi \leq \theta \leq k\pi$, where $k = 1, 2, \dots, 8$. The phase composites are constructed by averaging the given field over all θ in the phase interval k , for the entire time. The statistical significance of the MSSA eigenmodes was determined by following the Monte Carlo test against signals from red noise (Allen and Robertson 1996; Allen and Smith 1996).

3 The extra-tropical oscillations

The eigenmode pairs (4, 5), (6, 7) and (16, 17) emerge as three distinct oscillatory modes from the MSSA decomposition. The statistical significance of all the three pairs of the oscillatory modes passed 1% significance level, i.e., each eigenvalue lies above the 99.99th percentile of the corresponding surrogate Monte-Carlo distributions. The power spectra of these oscillatory modes are shown in Fig. 2a. The spectra of each pair are almost identical, and those of different pairs are distinct. The broadness of the spectra indicates that the oscillations are nonlinear while the central or peak values are the average periods. These three oscillatory modes have average periods of 120, 45 and 28 days, and will be referred to as the mid-latitude seasonal oscillation (MLSO), mid-latitude ISO-1 (MLISO-1), and mid-latitude ISO-2 (MLISO-2), respectively. They are listed in Table 1, along with their main characteristics. The two eigenmodes of each pair are combined to construct an oscillation, which by construction has propagating characteristics, and their RCs are constructed. Each RC is the decomposition of the original time series and will be referred to simply as oscillation hereafter. The spatial distribution of standard deviation of the oscillations (Fig. 2b) shows that the maximum value is around 12% of the standard deviation of the total daily anomalies for each oscillation. The area of maximum value decreases from MLSO to MLISO-2. The location of maximum centers varies from oscillation to oscillation. Notable regions of large values are in the North Atlantic for MLSO, North America and Northern Europe for MLISO-1 and Alaska for MLISO-2.

Plaut and Vautard (1994) also identified a pair of eigenmodes corresponding to an oscillation of about 120 days, which they characterized as the third harmonic of the annual cycle. The period of MLISO-1 is similar to the 40–45-day oscillation identified by Plaut and Vautard (1994) by applying MSSA to the Atlantic sector extending from 30° N to 70° N and 80° W to 40° E with a lag window of 200 days, the Pacific sector (30° N– 70° N, 140° E– 10° W) and the NH extra-tropics with an 80-day lag window, respectively. The 40–45-day oscillation over the Atlantic is not found when MSSA is applied to the global domain with the lag window of 200 days.

A spatial EOF analysis of each oscillation provides the spatial structure and the time evolution of the corresponding oscillation. Figure 3 shows the first EOF and first PC of each oscillation. The first PC denotes the index of the oscillation whereas the first EOF characterizes the spatial pattern of the oscillatory mode. The spatial patterns suggest that MLSO (Fig. 3a) projects onto the canonical pattern of NAO (Wallace and Gutzler 1981) or AO

Fig. 2 Spectra and standard deviation of oscillatory modes. **a** Power spectra of the two RCs of MLSO (blue), MLISO-1 (green), and MLISO-2 (red). Standard deviation of the RCs (as percentage of the standard deviation of the total anomalies) of **b** MLSO, **c** MLISO-1, and **d** MLISO-2

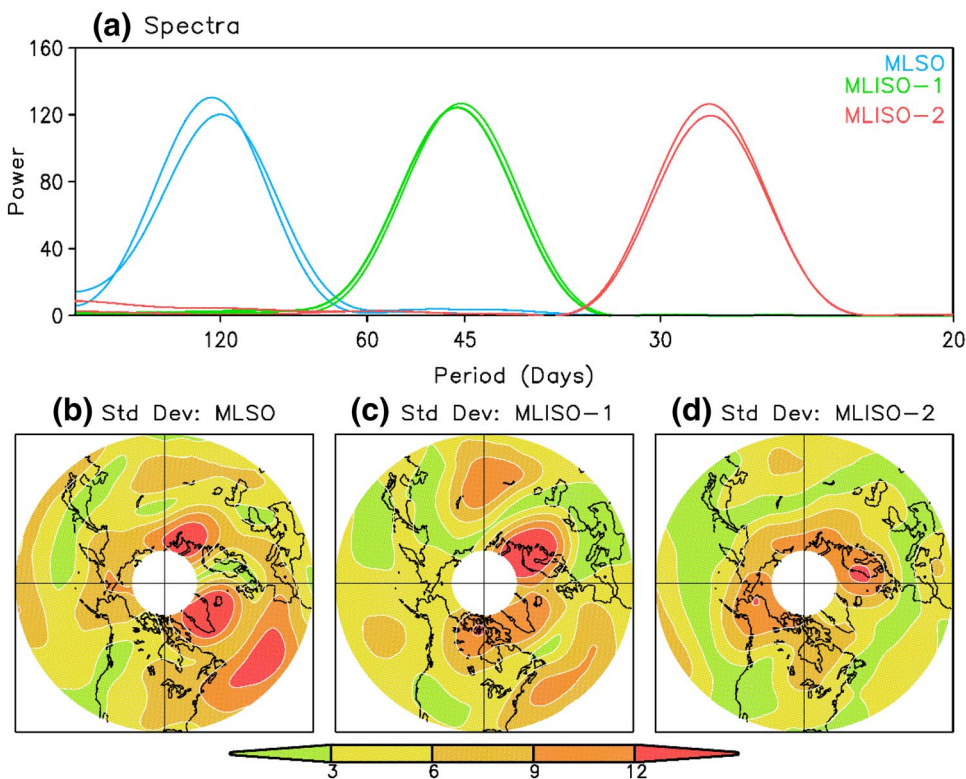


Table 1 Characteristics of oscillatory pairs identified by MSSA of Z500 daily anomaly over the extra-tropical Northern Hemisphere 30°N and 80°N using a lag window of 241 days

Oscillation/(MSSA pair)	Period (days)	Variance (%)	Propagation characteristics	Centers of action
MLSO/(4–5)	120	0.6	Westward: 3–4 m/s westward of 120°W	North Atlantic dipole connected to anomalies over Eurasia and N. Pacific
MLISO-1/(6–7)	45	0.5	Westward: 3 m/s in high-latitudes 10–12 m/s mid-latitudes	N. Pacific and N. Atlantic oriented in NW–SE direction
MLISO-2/(16–17)	28	0.4	20 m/s around the globe	Positive (negative) over Alaska and negative (positive) over Eastern Canada and Northern Europe

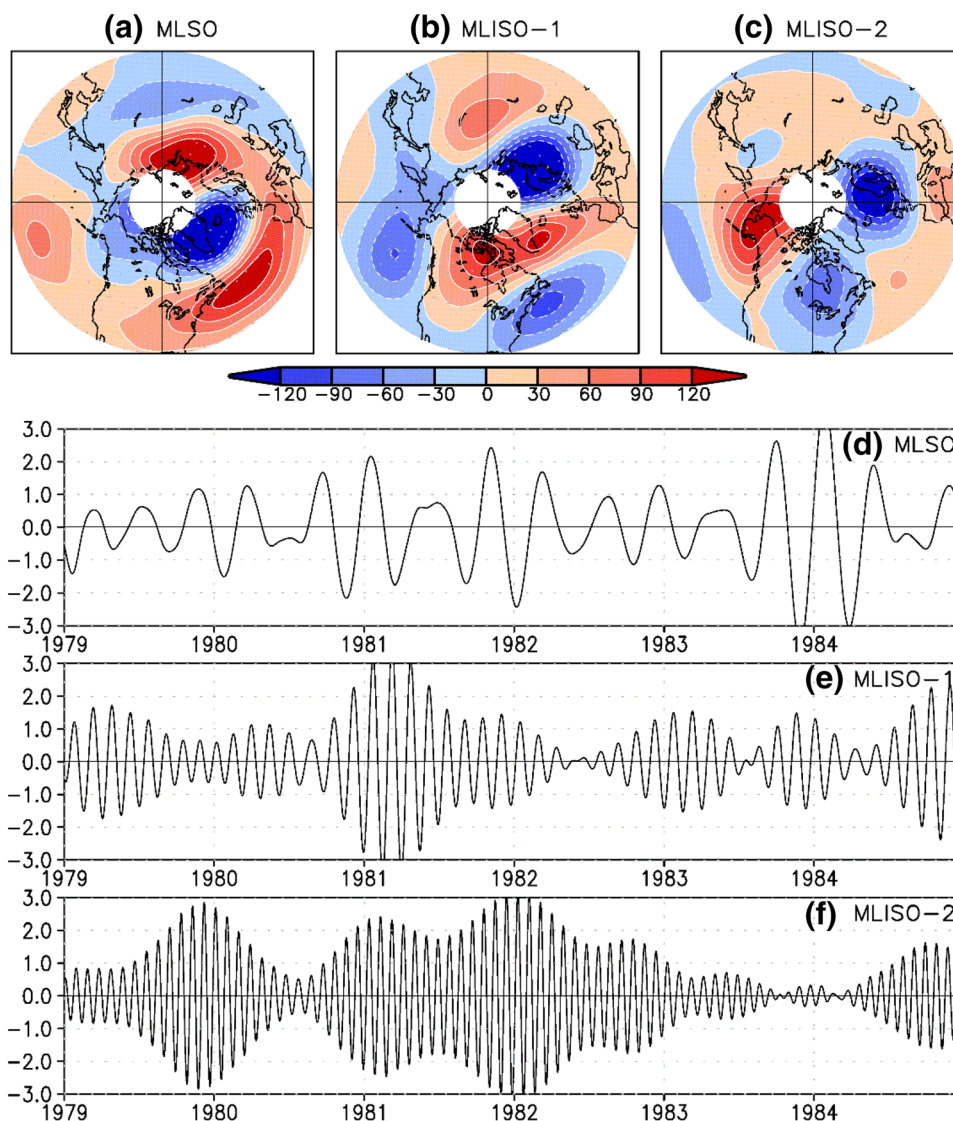
The period represents the mean value of the spectral band. The variance explained is computed from the eigenvalue spectrum

(Thompson and Wallace 1998) and MLISO-1 resembles the PNA pattern (Fig. 3b). However, a comparison of the life cycle of mid-latitude oscillations to the canonical teleconnection patterns does not support a one-to-one correspondence (Figs. 4, 5). While in some phases the mid-latitude oscillations are highly correlated with the canonical patterns in other phases the correlation is very weak. The correspondence between the 120- and 45-day oscillations and the canonical teleconnection patterns is investigated by comparing the phase composites of the 500-hPa geopotential height anomalies associated with MLSO to NAO and AO (Fig. 4) and MLISO-1 to the PNA pattern.

The geopotential height anomalies corresponding to the canonical patterns are obtained as the orthogonal projections

of the daily anomalies of 500-hPa geopotential height onto the corresponding daily teleconnection index. The daily NAO, AO and PNA teleconnection indices are calculated by the NOAA/CPC using the rotated principal component analysis (RPCA) method of Barnston and Livezy (1987) and were downloaded from ftp.cpc.ncep.noaa.gov. In this method monthly teleconnection patterns are computed for all months and then interpolated to the day in question. The NAO pattern extracted using the RPCA method contains a strong center over Greenland with centers of opposite sign over the Atlantic, Europe and the U.S. The PNA pattern has a strong center south of the Aleutian Islands, a center of opposite sign near the U.S.-Canadian border between the Pacific Ocean and Rocky Mountains, and a center of the

Fig. 3 Space-time structure of the oscillations. EOF1 of the RC of **a** MLSO, **b** MLISO-1, and **c** MLISO-2 and PC1 of the RC of **d** MLSO, **e** MLISO-1, and **f** MLISO-2. For clarity, PC1 is shown only for the period 1979–1985



same sign like the Aleutian center near the southeastern United States. A fourth center of sign opposite to that of the Aleutian center appears to its south near 20–30°N. The AO pattern has a center over the polar cap and two centers of opposite sign to that over the polar cap over the North Pacific Ocean and North Atlantic Ocean. These patterns show pronounced seasonal variation.

The NAO, AO, and PNA teleconnection indices are first filtered with a Lanczos band-pass filter (Duchon 1979). The filter applied to the NAO and AO indices has the half-power frequencies at $(90 \text{ day})^{-1}$ and $(120 \text{ day})^{-1}$, and the band-pass filter applied to the PNA teleconnection index has the half-power frequencies at $(30 \text{ day})^{-1}$ and $(90 \text{ day})^{-1}$. This filtering is intended to isolate the variability of the canonical patterns similar to the variability of the mid-latitude oscillations. The geopotential height anomalies associated with the NAO and AO are composited based on the phases of MLSO (Fig. 4) and the geopotential height anomalies associated with the

PNA are composited based on the phases of MLISO-1 (Fig. 5). Phases 2–3 and 6–7 of the MLSO show a high correlation with both NAO and AO whereas phases 4 and 8 show the lowest correlation between the MLSO and the canonical patterns. Phase 2 and 6 of the MLISO-1 show the largest correlation with the PNA and again phases 4 and 8 show the weakest correlation. The lack of correlation in the transition phases suggests that canonical teleconnection do not represent the transition between the positive and negative phase of the oscillations, and this result is consistent with Lee (2016) who argues that these teleconnection indices do not describe teleconnections as continuous variables.

The time variability of the mid-latitude oscillations (Fig. 3d, f) reflects their periods seen earlier in the spectra (Fig. 2a) and also shows seasonal modulation with higher amplitude during the boreal winter. The index of each oscillation can be reproduced by first projecting the daily anomalies of geopotential height onto the eigenmode pairs and

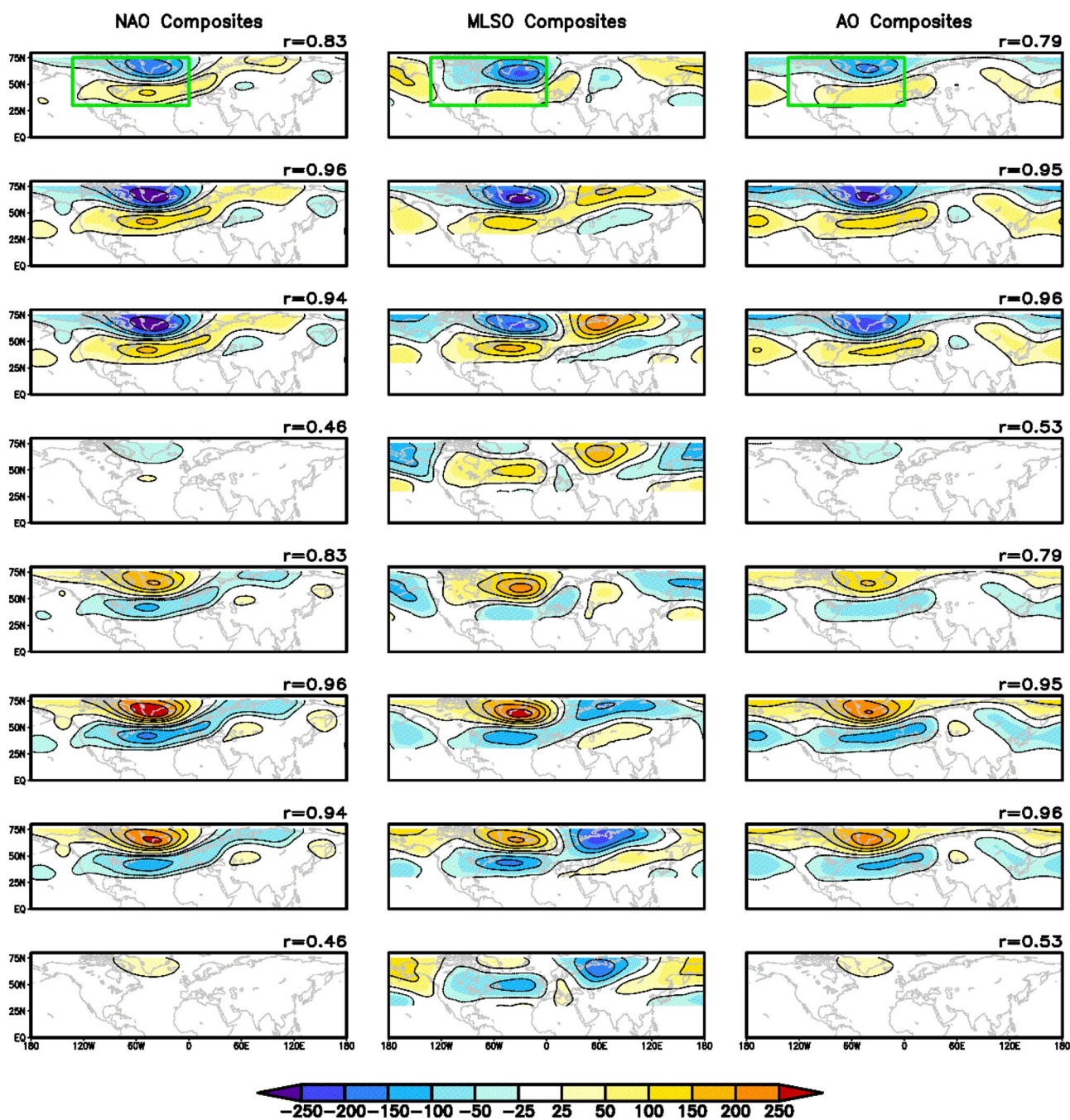


Fig. 4 Phase composites of geopotential height based on the MLSO. Phase composites of the NAO anomalies of 500-hPa geopotential height (left column), total daily anomalies of 500-hPa geopotential height (middle column), and AO anomalies of the 500-hPa geopotential height (right column). The correlation coefficient between the MLSO and canonical patterns over the region marked by the green box is indicated for each of the eight phases of MLSO. The correlation coefficient is significant at 95% confidence level

to the first half except that the anomalies are of opposite sign. The oscillations are global in the zonal direction and display propagating characteristics. The MLSO is characterized by a zonal wavenumber 1 pattern and propagates westward (Fig. 6a). A prominent feature of MLSO is the dipole structure in the North Atlantic, similar to the NAO

secondly by projecting the resulting timeseries of maps onto the corresponding spatial EOF.

The space–time structures of the oscillations are examined by decomposing each oscillation in eight phases. The phase composites are shown in Fig. 6 for the first half cycle of each oscillation. The second half cycle is almost identical

to the first half except that the anomalies are of opposite sign. The oscillations are global in the zonal direction and display propagating characteristics. The MLSO is characterized by a zonal wavenumber 1 pattern and propagates westward (Fig. 6a). A prominent feature of MLSO is the dipole structure in the North Atlantic, similar to the NAO

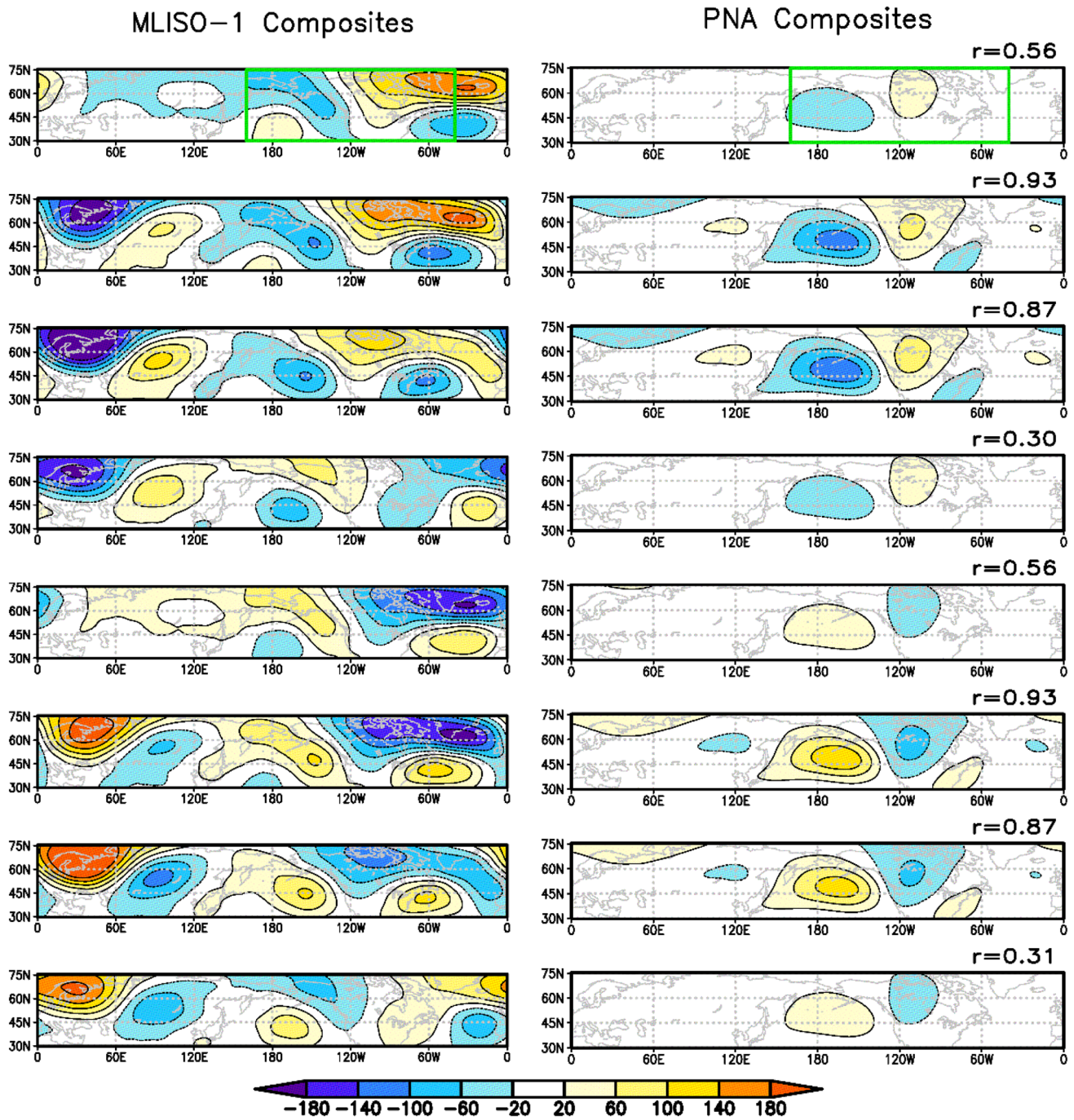


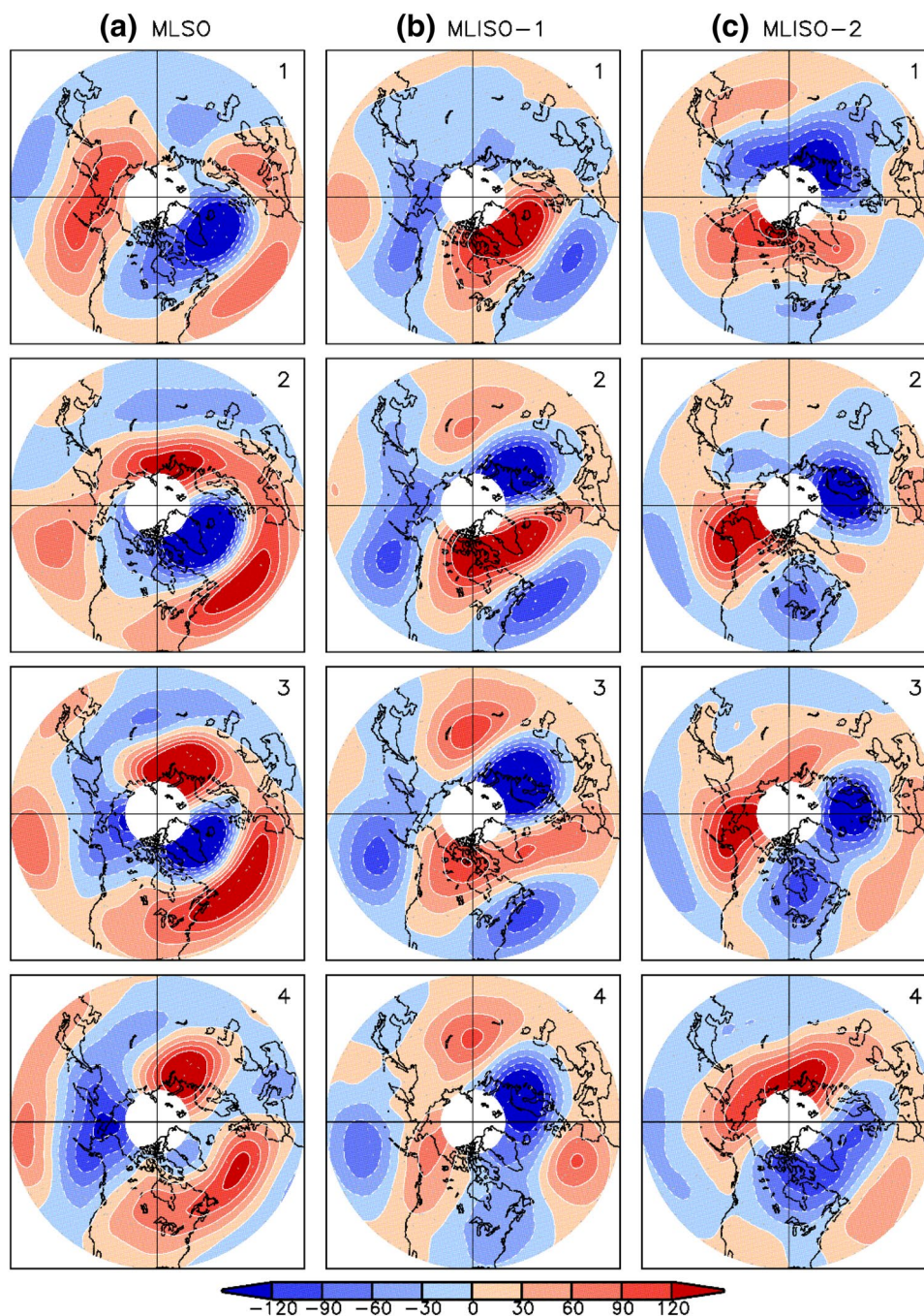
Fig. 5 Phase composites of geopotential height based on the MLISO-1. Phase composites of the PNA anomalies of 500-hPa geopotential height (left column) and total daily anomalies of 500-hPa geopotential height (right column). The correlation coefficient between the

MLISO-1 and PNA over the region marked by the green box is indicated for each of the eight phases of MLISO-1. The correlation coefficient is significant at 95% confidence level

pattern, which amplifies and expands in phases 2 and 3. The North Atlantic pattern is also connected to anomalies in Eurasia and Northern Pacific. The MLISO-1 exhibits a zonal wavenumber 2 pattern with a dipole over North America and North Atlantic oriented in northwest-southeast direction (Fig. 6b). In phases 2 and 3, the positive anomalies

are present over the western U.S. and Canada and negative anomalies over the eastern U.S., resembling the PNA pattern. When the domain is restricted to the Pacific sector, Plaut and Vautard (1994) describe the 40–45-day oscillation as a monopole pattern drifting westward with amplitude and phase speed varying as function of the oscillation’s phase. In

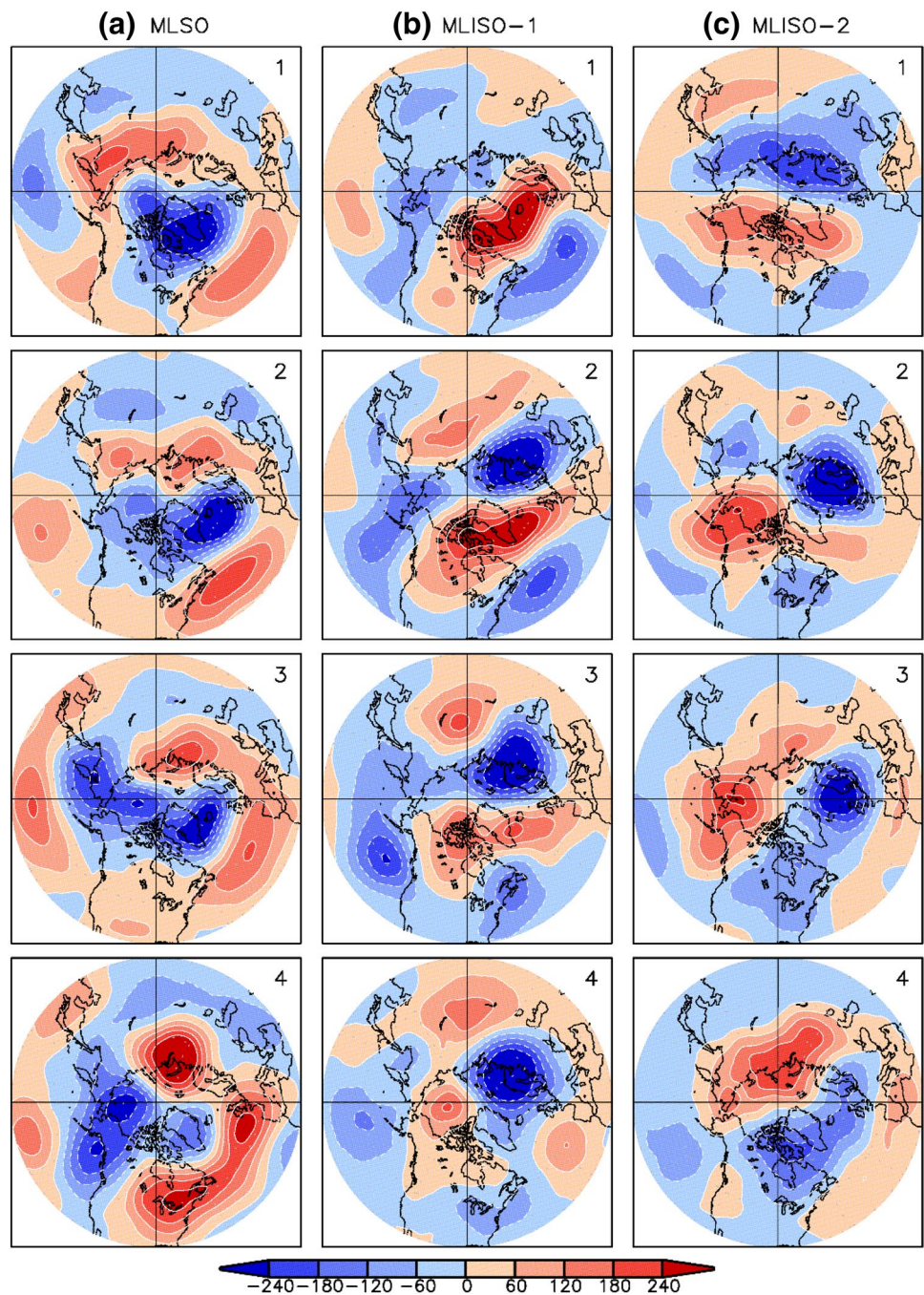
Fig. 6 Phase composites of the oscillations. Phase composites of the RC of **a** MLSO, **b** MLISO-1, and **c** MLISO-2 for the first half cycle of the corresponding oscillation. Each phase is of length $\pi/4$ and the phase number is indicated in the top right corner in each panel



phases with maximum amplitude, the oscillation is almost a standing wave and projects onto PNA. When the analysis is extended to the NH extra-tropics the 40–45-day oscillation shows a reduced amplitude over the Pacific domain and enhancement of the Atlantic jet stream east of its average position. They suggest that the Atlantic pattern results from the phase locking between the 40 and 45-day oscillation over the Pacific and a 30–35-day oscillation specific to the North Atlantic, oscillation that tends to favor the occurrence of Euro-Atlantic blocking.

The MLISO-2 is also characterized by a zonal wavenumber 1 pattern that is confined mainly to higher latitudes and moves westward (Fig. 6c). During the peak phases 2 and 3, maximum positive anomalies are seen over the Alaska and adjoining regions along with negative anomalies over eastern Canada and northern Europe, reminiscent of the Alaskan ridge pattern (Straus et al. 2007). The corresponding phase composites with total anomalies of the 500-hPa geopotential height (Fig. 7) show a good resemblance to the phase composites of the oscillations (Fig. 6) for all the three oscillations

Fig. 7 Phase composites of geopotential height. Phase composites of the total anomalies of 500-hPa geopotential of **a** MLSO, **b** MLISO-1, and **c** MLISO-2 for the first half cycle of the corresponding oscillation. Each phase is of length $\pi/4$ and the phase number is indicated in the top right corner in each panel

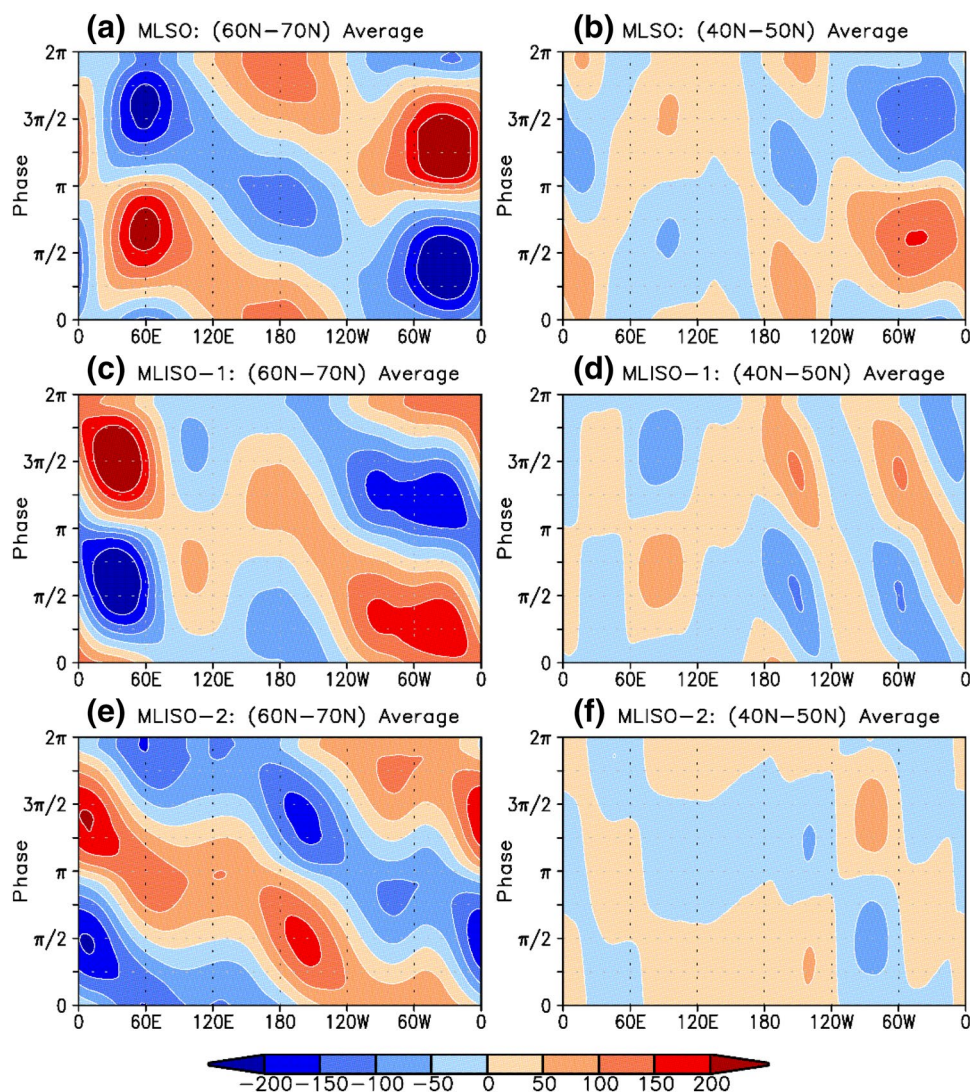


but with twice the magnitude. This correspondence indicates that the oscillations are robust features embedded in the daily variability of the geopotential height at proper phases.

The zonal and meridional propagation of the oscillations is examined through latitude-phase cross-sections and longitude-phase cross-sections. The MLSO propagates westward to the west of 120°W with a phase speed of 3–4 m/s and shows a standing pattern to the east of 120°W at higher latitudes, while no propagation is evident in mid-latitudes (Fig. 8a, b). The MLISO-1 exhibits westward propagation to the east of the dateline and a standing pattern to the west

of the dateline (Fig. 8c, d). The phase speed in the high-latitudes is about 3 m/s and about 10–12 m/s in the mid-latitudes. The MLISO-2 propagates westward around the globe at higher latitudes with a phase speed of about 20 m/s and shows negligible presence or movement in the mid-latitudes (Fig. 8e, f). The MLSO propagates northward over the North Atlantic and North America (Fig. 9a, b) while MLISO-1 shows standing patterns in both these regions (Fig. 9c, d). The MLISO-2 propagates northward over the North Atlantic and has a standing pattern over North America (Fig. 9e, f). These results are summarized in Table 1.

Fig. 8 Zonal propagation of the oscillations. Longitude-phase cross-sections of the MLSO RC averaged over **a** 60°N–70°N, **b** 40°N–50°N, MLISO-1 RC averaged over **c** 60°N–70°N, **d** 40°N–50°N, and MLISO-2 RC averaged over **e** 60°N–70°N, **f** 40°N–50°N



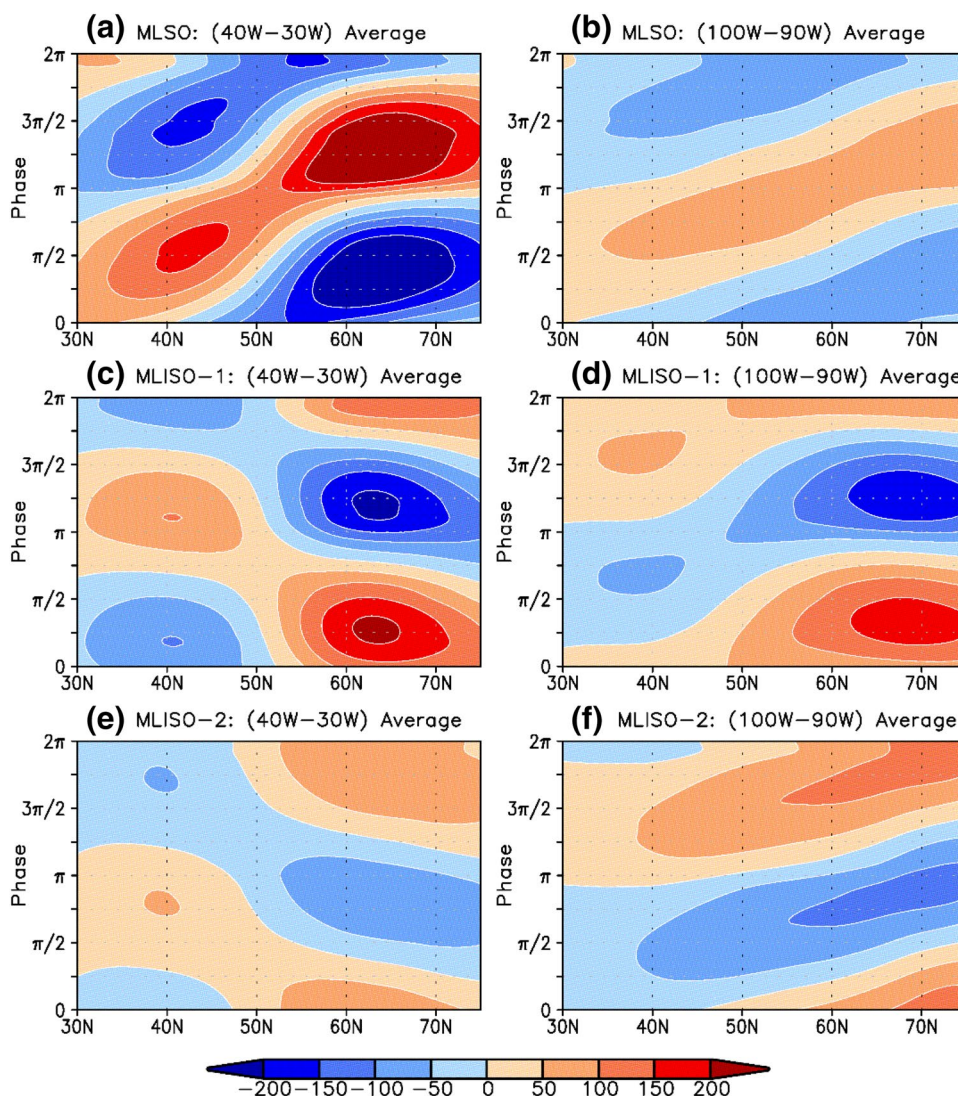
The dynamical features of the oscillations can be understood by examining the phase composites of surface pressure, surface temperature, and low-level wind. For example, during the peak phase 2, the MLSO exhibits a surface pressure dipole over the North Atlantic (Fig. 10a), which is accompanied by cold (warm) surface temperature anomalies (Fig. 11a) and anticyclonic (cyclonic) wind at low-level (Fig. 12a) to the north (south). This surface pressure dipole is maintained over the entire half-cycle of the oscillation but expands and propagates (Fig. 10a) while the surface temperature also shows movement of warm anomalies over to the North American continent (Fig. 12a). In phase 2, the MLISO-1 shows low pressure and cold anomalies over the Atlantic and eastern U.S. and high pressure (Fig. 10b) and warm anomalies (Fig. 11b) over the northwest part of North America. These temperature and pressure anomalies are accompanied by cyclonic (anticyclonic) circulation in the east (west) (Fig. 12b). During the whole half-cycle (Figs. 10b, 11b), the surface pressure, and surface

temperature patterns propagate westward to some extent. The MISO-2 reveals a strong high-pressure system over the Alaskan region in phase 2 (Fig. 10c), accompanied by warm anomalies over Alaska and cold anomalies to the southeast (Fig. 11c) and cyclonic flow over the Alaskan region (Fig. 12c). Over the whole half-cycle, the surface pressure propagates westward over the high-latitudes (Fig. 10c) while the surface temperature reveals a cold effect over North America (Fig. 11c). Thus, the three oscillations show dynamically consistent relations.

4 Potential predictability of mid-latitude oscillations

The signals of mid-latitude oscillations detected in the surface pressure, temperature, and wind suggest that these oscillations can represent a source of predictability for intra-seasonal time scales. This is assessed using a multivariate

Fig. 9 Meridional propagation of the oscillations. Latitude-phase cross-sections of the MLSO RC averaged over **a** 40°W–30°W, **b** 100°W–90°W, MLISO-1 RC averaged over **c** 40°W–30°W, **d** 100°W–90°W, and MLISO-2 RC averaged over **e** 40°W–30°W, **f** 100°W–90°W



regression model with the index of each mid-latitude oscillation, shown in Fig. 3d–f, as one of the predictors. The linear regression model is adopted from Rodney et al. (2013) and predicts the temperature anomaly based on a combination of current and past (one pentad in the past) MJO states defined by the principal components (PCs) of RMM Index (Wheeler and Hendon 2004), and current temperature anomaly. The predictand is the 2-m temperature at four future pentads, $T(t)$. The model can be written as:

$$T(t) = a_1(t)PC1(0) + a_2(t)PC1(-1) + b_1(t)PC2(0) + b_2(t)PC2(-1) + c(t)T(0) + d(t)X(0)$$

where $t = 1, 2, 3, 4$ represent the forecast pentads, $\{a_1(t), a_2(t), b_1(t), b_2(t), c(t), d(t)\}$ are the regression coefficients to be solved for. $X(0)$ denotes one of the midlatitude oscillation indices corresponding to the current state, and $T(0)$ represents the current state of 2-m temperature. The

version of the model without the midlatitude oscillation as a predictor is referred to as the 2-predictor model and the version of the model with one of the midlatitude oscillations as a predictor is referred to as the 3-predictor model. The 2-predictor model is the same model as in Rodney et al. (2013).

The regression coefficients are calculated using the linear least-square fitting method on a reduced dataset corresponding to the period 1996–2012. The regression model is then used to forecast the 2-m temperature for the period 1979–1995. The forecast skill of the model, measured by the anomaly correlation between the predicted and observed 2-m temperature during 1979–1995 is shown in Figs. 13, 14, 15, 16. Figure 13 shows the anomaly correlation of the 2-predictor version of the model and the skill is comparable to results of Rodney et al. (2013), which is applied only to boreal winter. Figures 14, 15, 16 show the anomaly correlation of the 3-predictor version of the model, where the third predictor corresponds MLISO-2 (Fig. 14), MLISO-1

Fig. 10 Phase composites of surface pressure. Phase composites of surface pressure (hPa) for **a** MLSO, **b** MLISO-1 and **c** MLISO-2 for half a cycle of the corresponding oscillation. Each phase is of length $\pi/4$ and the phase number is indicated in the top right corner in each panel

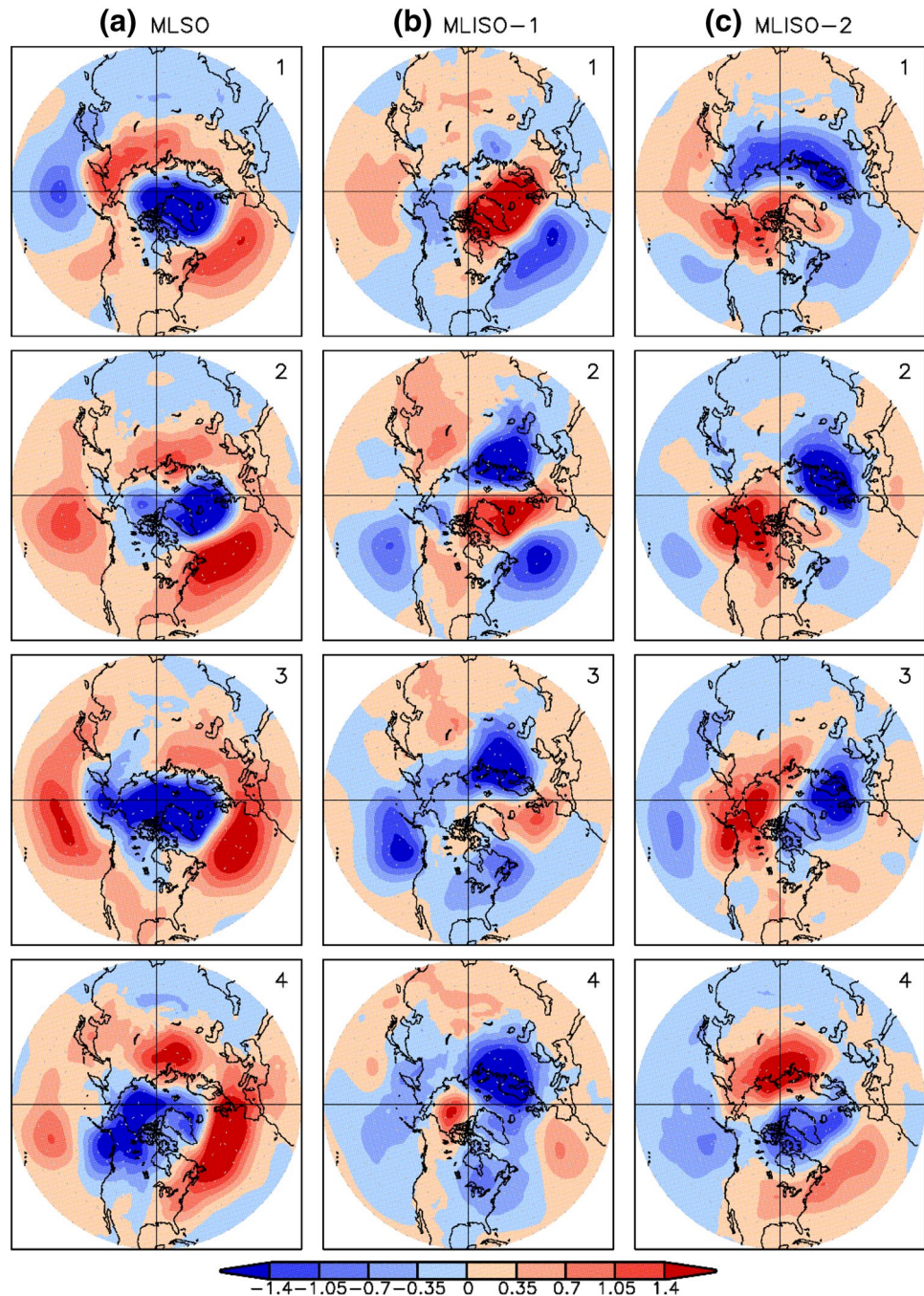
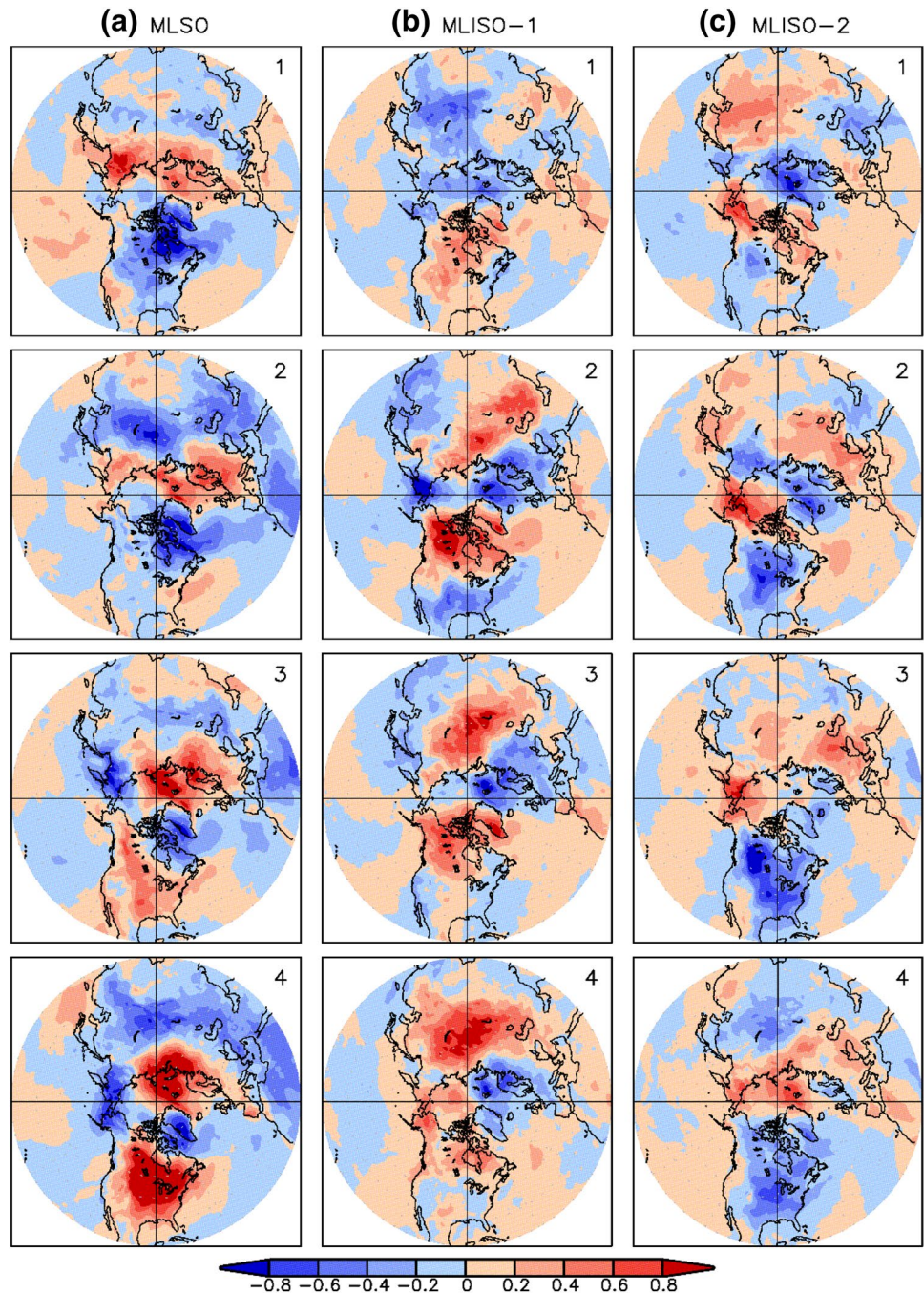


(Fig. 15), and MLSO (Fig. 16). The inclusion of mid-latitude oscillations increases the accuracy of forecast at longer leads. All oscillations enhance the forecast skill of the 2-predictor model over the transection extending from the eastern seaboard of U.S. to the Canadian prairies and into Alaska. In addition, each oscillation shows particular regions of influences. For example, the influence of MLISOs on the southern U.S. is not statistically significant by pentad 4 whereas MLSO has a small but significant influence. MLISO-1 has a larger influence on the Upper Midwest and Plains, whereas

the influence of MLISO-2 and MLSO is stronger in the Ohio Valley.

The skill score based on the mean-square-error (Murphy 1988) shows an improvement in the forecast skill of the 3-predictor model by 5-10% at the 4th pentad relative to the 2-predictor model (Fig. 17) for all oscillations. In the eastern side of Ohio Valley and western Mid-Atlantic the 3-predictor model shows a decrease in the skill score, and the area of the region with a degradation in skill decreases as the time scale of the midlatitude oscillation gets longer. The predictive skill

Fig. 11 Phase composites of surface temperature. Phase composites of surface temperature (K) for **a** MLSO, **b** MLISO-1, and **c** MLISO-2 for half a cycle of the corresponding oscillation. Each phase is of length $\pi/4$ and the phase number is indicated in the top right corner in each panel



of the model perhaps might be further improved with a better understanding of the delayed and/or prolonged impact of these oscillations on the surface air temperature variability.

Given the resemblance between some phases of the mid-latitude oscillations and canonical teleconnection patterns, the latter were used as predictors in the linear regression model. Figure 18 shows the forecast skill of the 3-predictor model at pentad 4 using each of the teleconnection patterns as a predictor. While there are similarities between the forecast skill of the 3-predictor model using as predictors

the midlatitude oscillations and teleconnection patterns, respectively, a few differences are notable. First, a comparison between the impact of PNA (Fig. 18a) and MLISO-1 (Fig. 15d) shows a better skill in the southeastern and northwestern U.S. for the version of the model based on MLISO-2. Second, the forecast skill of the model based on MLSO picks up the strengths of both NAO and AO predictors. The anomaly correlation of MLSO (Fig. 16d) is slightly better than the skill of AO over the southeastern part of the U.S.

Fig. 12 Relation with low-level horizontal wind. Phase 2 composites of 850-hPa horizontal wind (m s^{-1}) for **a** MLSO, **b** MLISO-1, and **c** MLISO-2

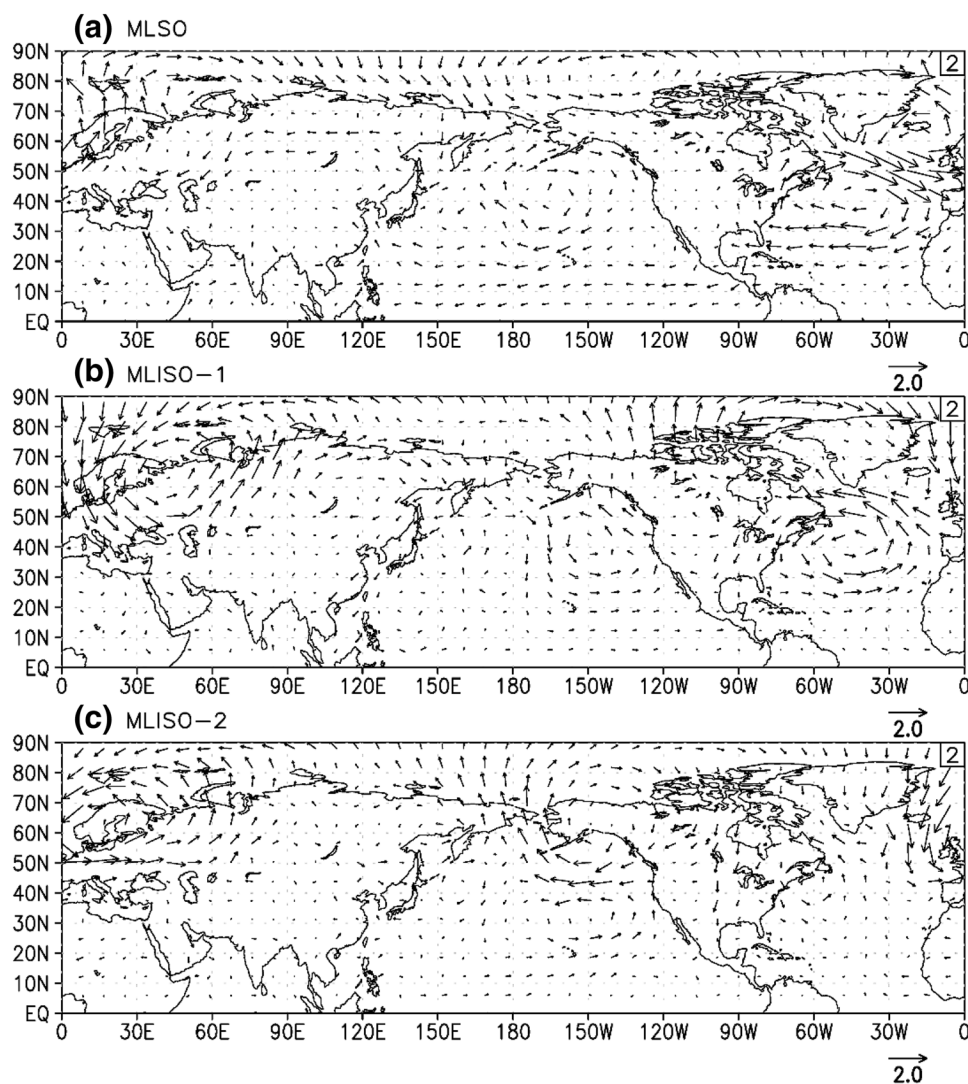


(Fig. 18b) and slightly better than the skill of NAO over the northwestern U.S. (Fig. 18c).

5 Summary and conclusions

This study has established the existence of at least three nonlinear oscillations in the NH extra-tropics, MLSO, MLISO-1, and MLISO-2, and has described the detailed space–time structures of these oscillations on daily time scale. The importance of these oscillations is brought about by their significant standard deviation, statistical significance, distinct features, and their relations with the well-known phenomena such as NAO and PNA. The oscillatory behavior of these modes, although nonlinear, implies higher predictability at longer time scale. Since these oscillations occur in the intra-seasonal and seasonal time scales, they provide a basis for bridging weather and climate predictions.

The nonlinear empirically constructed modes found in this study offer a basis for long-range prediction of climate in the midlatitude. There is potential to exploit the near-regular behavior of these oscillations for predicting certain aspects of the mid-latitude climate at long lead time, similar to the attempts made in predicting the MJO and monsoon intra-seasonal oscillations in the tropics. The extension of a multilinear regression model based on the principal components that characterizes MJO and persistence to include the current state of the extra-tropical oscillations shows an improved forecast skill at longer lead times.

Suggestions for future research include the physical mechanisms driving these oscillations, the teleconnection patterns associated with the oscillations, their relationship with other intraseasonal modes of variability, e.g., global wind oscillation (Weickman and Berry 2007, 2009), and the predictions of meteorological parameters over the areas influenced by these oscillations.

Fig. 13 Correlation coefficient between observed and forecasted 2-m temperature anomaly with lead times of **a** 1, **b** 2, **c** 3, and **d** 4 pentads during 1979–1995. The linear regression model is based on two predictors: MJO and current temperature. Shading represents areas where the correlation coefficient is statistically significant at the 0.05 level

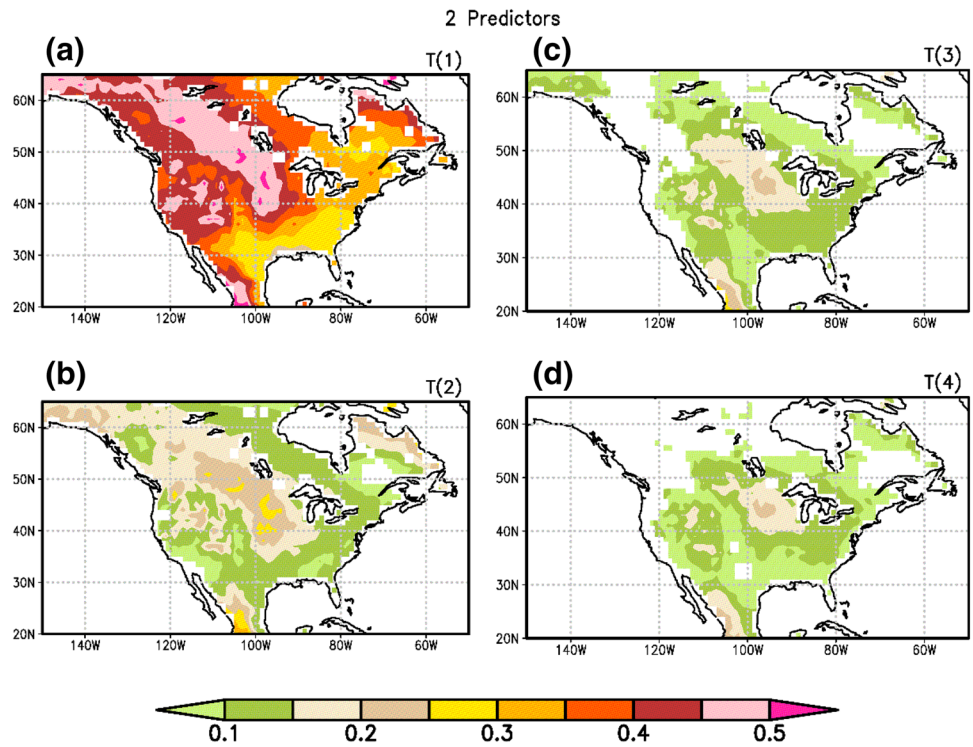


Fig. 14 Correlation coefficient between observed and forecasted 2-m temperature anomaly with lead times of **a** 1, **b** 2, **c** 3, and **d** 4 pentads during 1979–1995. The linear regression model is based on three predictors: MJO, current temperature, and MLISO-2. Shading represents areas where the correlation coefficient is statistically significant at the 0.05 level

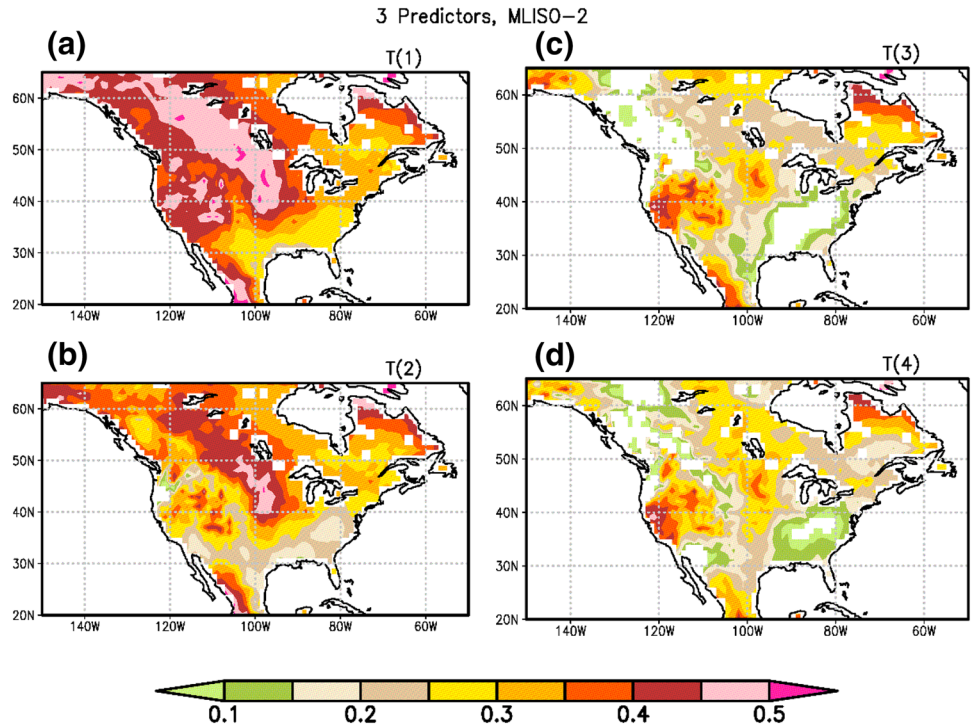


Fig. 15 Same as Fig. 14 except for MLISO-1

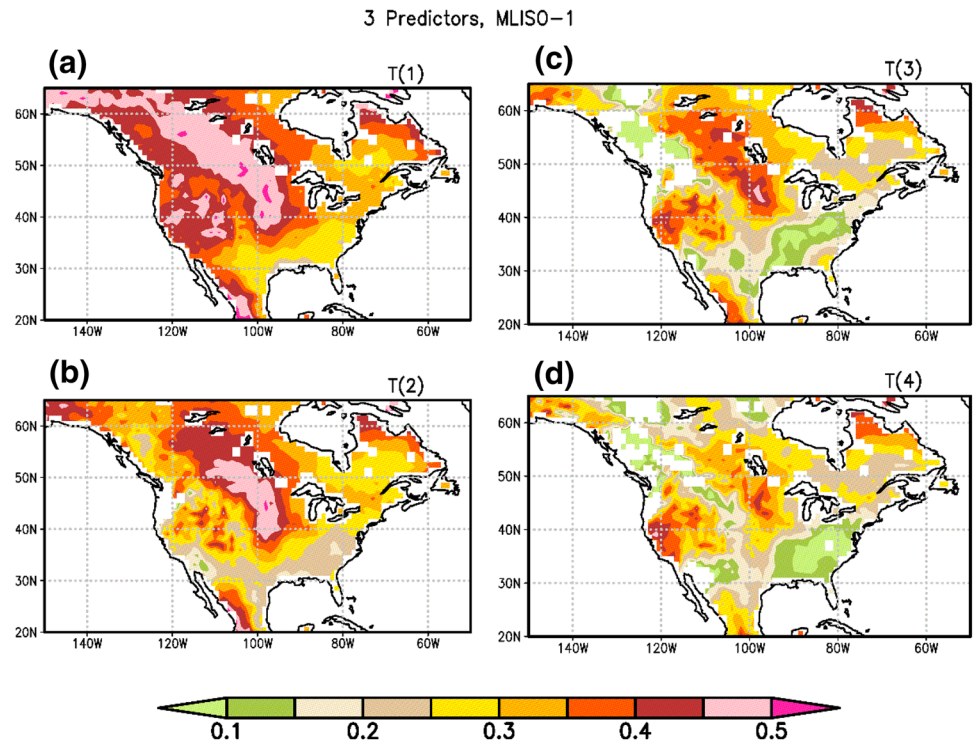
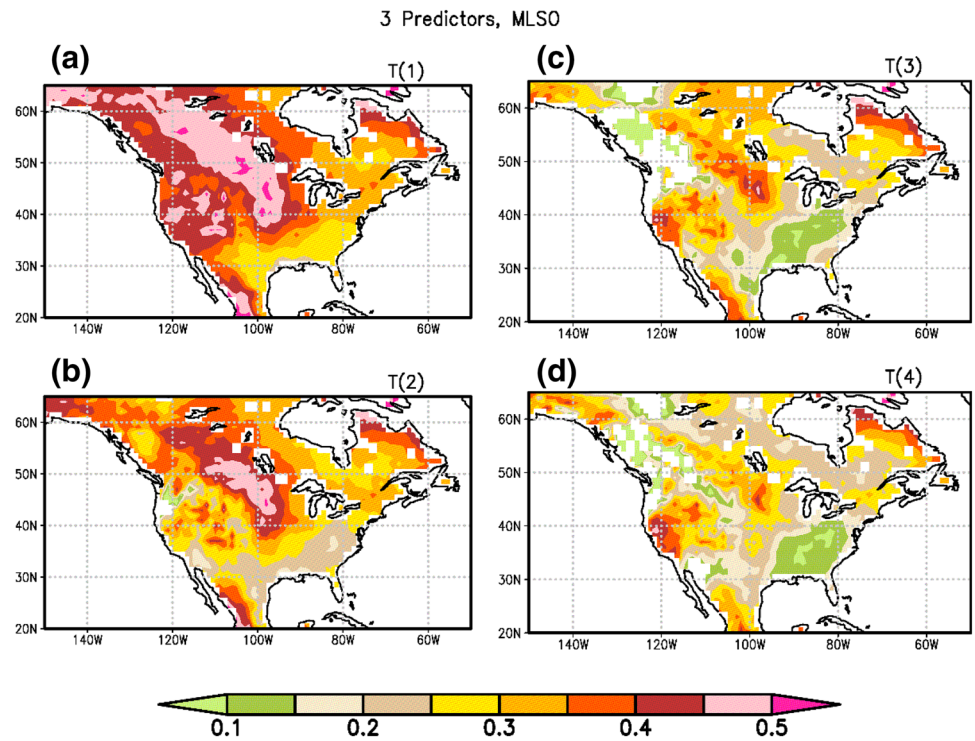


Fig. 16 Same as Fig. 14 except for MLSO



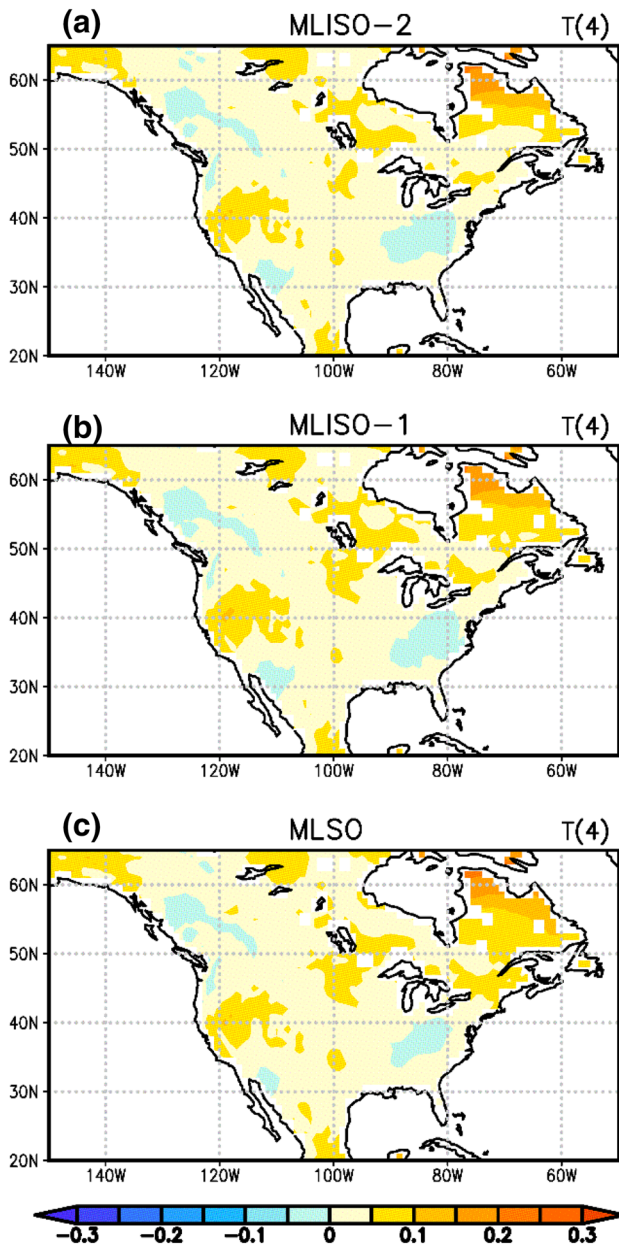


Fig. 17 Mean absolute error skill score of the 2-m temperature anomaly forecast at pentad 4 during 1979–1995 using **a** MLISO-2, **b** MLISO-1, and **c** MLSO as a predictor in the 3-predictor regression model

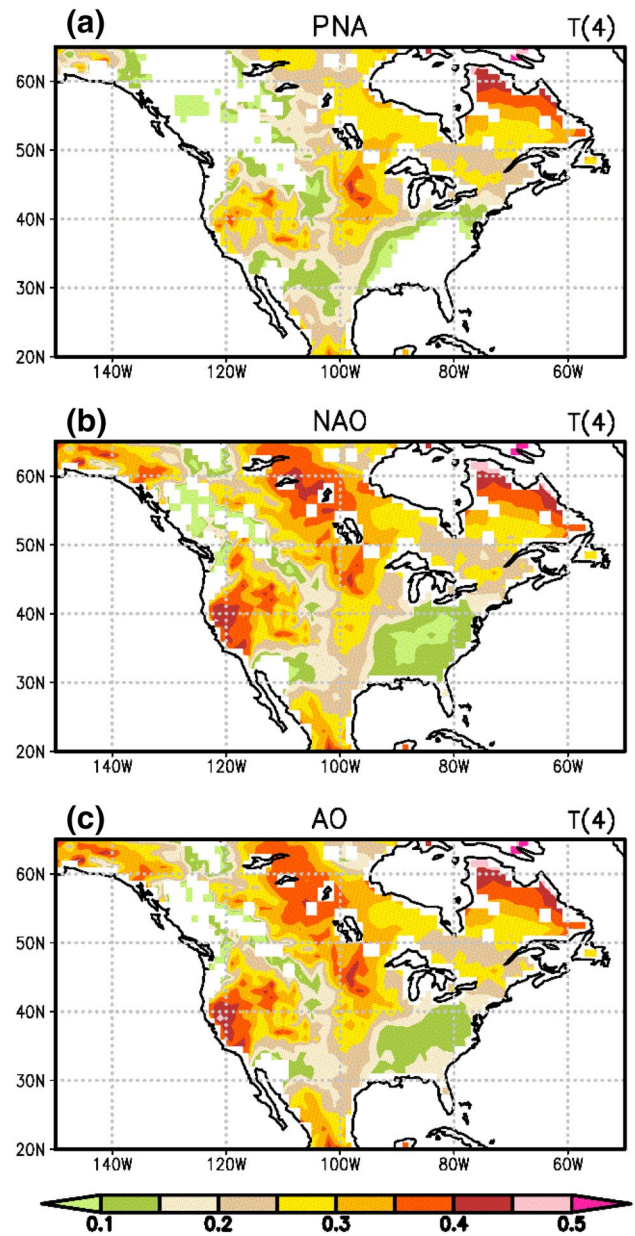


Fig. 18 Correlation coefficient between observed and forecasted 2-m temperature anomaly at lead time 4 pentads during 1979–1995. The 3-predictor linear regression model uses **a** PNA, **b** NAO, and **c** AO as one of the predictors. Shading represents areas where the correlation coefficient is statistically significant at the 0.05 level

Acknowledgements C.S. was supported by US NOAA, Grant NA16NWS4680022. V.K. was supported by the US NSF (grant AGS-133A8427), US NOAA (grant MAPP-NA14OAR4310160), US NASA (grant NNX14AM19G).

Compliance with ethical standards

Conflict of interest The authors declare no conflict of interest.

References

- Allen MR, Robertson AW (1996) Distinguishing modulated oscillations from coloured noise in multivariate datasets. *Clim Dyn* 12:775–784. <https://doi.org/10.1007/s003820050142>
- Allen MR, Smith LA (1996) Monte Carlo SSA: detecting irregular oscillations in the presence of colored noise. *J Clim* 9:3373–3404. [https://doi.org/10.1175/1520-0442\(1996\)009%3c3373:MCSDIO%3e2.0.CO;2](https://doi.org/10.1175/1520-0442(1996)009%3c3373:MCSDIO%3e2.0.CO;2)
- Barnston AG, Livezey RE (1987) Classification, seasonality and persistence of low-frequency atmospheric circulation patterns. *Mon Weather Rev* 115:1083–1126. [https://doi.org/10.1175/1520-0493\(1987\)115%3c1083:CSAPOL%3e2.0.CO;2](https://doi.org/10.1175/1520-0493(1987)115%3c1083:CSAPOL%3e2.0.CO;2)
- Branstator AG (2002) Circumglobal teleconnections, the jet stream waveguide, and the North Atlantic Oscillation. *J Clim* 15:1893–1910. [https://doi.org/10.1175/1520-0442\(2002\)015%3c1893:CTJJSW%3e2.0.CO;2](https://doi.org/10.1175/1520-0442(2002)015%3c1893:CTJJSW%3e2.0.CO;2)
- Dee DP, Uppala SM, Simmons AJ et al (2011) The ERA-Interim reanalysis: configuration and performance of the data assimilation system. *Quart J R Meteorol Soc* 137:553–597. <https://doi.org/10.1002/qj.828>
- Feldstein SB (2000) The time scale, power spectra, and climate noise properties of teleconnection patterns. *J Clim* 13:4430–4440. [https://doi.org/10.1175/1520-0442\(2000\)013%3c4430:TTPSA%3e2.0.CO;2](https://doi.org/10.1175/1520-0442(2000)013%3c4430:TTPSA%3e2.0.CO;2)
- Feliks Y, Ghil M, Robertson AW (2010) The atmospheric circulation over the North Atlantic as induces SST field. *J Clim* 24:522–542. <https://doi.org/10.1175/2010JCLI3859.1>
- Feliks Y, Robertson AW, Ghil M (2016) Interannual variability in North Atlantic weather: data analysis and a quasigeostrophic model. *J Atmos Sci* 73:3227–3248. <https://doi.org/10.1175/JCLI-D-16-0370.1>
- Franzke C (2009) Multi-scale analysis and teleconnection indices: climate noise and non-linear trend analysis. *Nonlin Proc Geophys* 16:65–76. <https://doi.org/10.5194/npg-16-65-2009>
- Franzke C, Feldstein SB (2005) The continuum and dynamics of the Northern Hemisphere teleconnection patterns. *J Atmos Sci* 62:3250–3267. <https://doi.org/10.1175/JAS3536.1>
- Gerber EP, Polvani LM, Ancukiewicz D (2008) Annular mode time scales in the intergovernmental panel on climate change fourth assessment report models. *Geophys Res Lett* 35:L22707. <https://doi.org/10.1029/2008GL035712>
- Ghil M, Mo K (1991) Intraseasonal oscillation in the global atmosphere. Part I: northern Hemisphere and tropics. *J Atmos Sci* 48:752–779. [https://doi.org/10.1175/1520-0469\(1991\)048%3c0780:IOITGA%3e2.0.CO;2](https://doi.org/10.1175/1520-0469(1991)048%3c0780:IOITGA%3e2.0.CO;2)
- Ghil M, Allen MR, Dettinger MD et al (2002) Advanced spectral methods for climate time series. *Rev Geophys* 40(1):1003. <https://doi.org/10.1029/2000RG000092>
- Gottschalck J, Wheeler M, Weickmann K et al (2010) A framework for assessing operational Madden-Julian Oscillation forecasts—A CLIVAR MJO working group project. *Bull Am Meteorol Soc* 91:1247–1258. <https://doi.org/10.1175/2010BAMS2816.1>
- Hasselmann K (1976) Stochastic climate models. Part I: Theory. *Tellus* 6:474–485. <https://doi.org/10.1111/j.2153-3490.1976.tb00696.x>
- Johnson NC, Feldstein SB (2010) The continuum of North Pacific sea level pressure patterns: intraseasonal, interannual, and interdecadal variability. *J Clim* 23:851–867. <https://doi.org/10.1175/2009JCLI3099.1>
- Kalnay E, Kanamitsu M, Kistler R et al (1996) The NCEP/NCAR 40-year reanalysis project. *Bull Am Meteorol Soc* 77:437–470
- Krishnamurthy V, Achuthavari D (2012) Intraseasonal oscillations of the monsoon circulation over South Asia. *Clim Dyn* 38:2335–2353. <https://doi.org/10.1007/s00382-016-3466-z>
- Krishnamurthy V, Shukla J (2007) Intraseasonal and seasonally persisting patterns of Indian monsoon rainfall. *J Clim* 20:3–20. <https://doi.org/10.1175/JCLI3981.1>
- Kushnir Y (1987) Retrograding wintertime low-frequency disturbances over the North Pacific. *J Atmos Sci* 44:2727–2742. [https://doi.org/10.1175/1520-0469\(1987\)044%3c2727:RWLFD%3e2.0.CO;2](https://doi.org/10.1175/1520-0469(1987)044%3c2727:RWLFD%3e2.0.CO;2)
- Kushnir Y, Robinson WA, Chang P, Robertson AW (2006) The physical basis for predicting Atlantic sector seasonal-to-interannual climate variability. *J Clim* 19:5949–5970. <https://doi.org/10.1175/JCLI3943.1>
- Lee CC (2016) Reanalysis the impacts of atmospheric teleconnections on cold-season weather using multi-variate surface weather types and self-organizing maps. *Int J Clim* 37:3714–3730. <https://doi.org/10.1002/joc.4950>
- Liebmann B, Smith CA (1996) Description of a complete (interpolated) outgoing longwave radiation dataset. *Bull Am Meteorol Soc* 77:1275–1277
- Mesinger F, DiMego G, Kalnay E et al (2006) North American regional reanalysis. *Bull Am Meteorol Soc* 87:343–360. <https://doi.org/10.1175/BAMS-87-3-343>
- Moron V, Vautard R, Ghil M (1998) Trends, interdecadal and interannual oscillations in global sea-surface temperatures. *Clim Dyn* 14:545–569. <https://doi.org/10.1007/s0038200502>
- Murphy AH (1988) Skill scores based on the mean square error and their relationship to the correlation coefficient. *Mon Weather Rev* 116:2417–2424. [https://doi.org/10.1175/1520-0493\(1988\)116%3c2417:SSBOTM%3e2.0.CO;2](https://doi.org/10.1175/1520-0493(1988)116%3c2417:SSBOTM%3e2.0.CO;2)
- National Academies of Sciences E. and Medicine (2016) Next generation Earth system prediction: strategies for subseasonal to seasonal forecasts. Washington, DC: The National Academies Press. <https://doi.org/10.17226/21873>
- Plaut G, Vautard R (1994) Spells of low-frequency oscillations and weather regimes in the Northern Hemisphere. *J Atmos Sci* 51:210–236. [https://doi.org/10.1175/1520-0469\(1994\)052%3c0210:solfoa%3e2.0.co;2](https://doi.org/10.1175/1520-0469(1994)052%3c0210:solfoa%3e2.0.co;2)
- Raynaud S, Yiou P, Kleeman R, Seich S (2005) Using MSSA to determine explicitly the oscillatory dynamics of weakly nonlinear climate systems. *Nonlin Proc Geophys* 12:807–815. <https://doi.org/10.5194/npg-807-2005>
- Rodney M, Lin H, Derome J (2013) Subseasonal prediction of wintertime North American surface air temperature during strong MJO events. *Mon Weather Rev* 141:2897–2909. <https://doi.org/10.1175/MWR-D-12-00221.1>
- Stan C, Straus DM, Frederiksen JS et al (2017) Review of tropical-extratropical teleconnections on intraseasonal time scales. *Rev Geophys* 55:902–937. <https://doi.org/10.1002/2016RG000538>
- Straus DM, Corti S, Molteni F (2007) Circulation regimes: chaotic variability versus SST-forced predictability. *J Clim* 20:2251–2272. <https://doi.org/10.1175/JCLI4070.1>
- Thompson DW, Wallace JM (1998) The Arctic oscillation signature in the wintertime geopotential height and temperature fields. *Geophys Res Lett* 25:1297–1300. <https://doi.org/10.1029/98GL00950>

- Thompson DWJ, Wallace JM (2000) Annular modes in the extratropical circulation. Part I: month-to-month variability. *J Clim* 13:1000–1016. [https://doi.org/10.1175/1520-0442\(2000\)013%3c1000:amitec%3e2.0.co;2](https://doi.org/10.1175/1520-0442(2000)013%3c1000:amitec%3e2.0.co;2)
- Vannitsem S, Ghil M (2017) Evidence of coupling in ocean-atmosphere dynamics over the north atlantic. *Geophys Res Lett* 44:2016–2026. <https://doi.org/10.1002/2016GL072229>
- Wallace JM, Gutzler DS (1981) Teleconnections in the geopotential height field during the Northern Hemisphere winter. *Mon Weather Rev* 109:784–812. [https://doi.org/10.1175/1520-0493\(1981\)109%3c0784:tiughf%3e2.0.co;2](https://doi.org/10.1175/1520-0493(1981)109%3c0784:tiughf%3e2.0.co;2)
- Weickmann K, Berry E (2007) A synoptic-dynamic model of subseasonal atmospheric variability. *Mon Weather Rev* 135:449–474. <https://doi.org/10.1175/MWR3293.1>
- Weickmann K, Berry E (2009) The tropical Madden-Julian Oscillation and the global wind oscillation. *Mon Weather Rev* 137:1601–1614. <https://doi.org/10.1175/MWR3293.1>
- Wheeler MC, Hendon HH (2004) An all-season real-time multivariate MJO index: development of an index for monitoring and prediction. *Mon Weather Rev* 132:1917–1932. [https://doi.org/10.1175/1520-0493\(2004\)132%3c1917:AARMMI%3e2.0.C;2](https://doi.org/10.1175/1520-0493(2004)132%3c1917:AARMMI%3e2.0.C;2)
- Wunsch C (1999) The interpretation of short climate records, with comments on the North Atlantic and Southern Oscillations. *Bull Am Meteorol Soc* 80:245–255. [https://doi.org/10.1175/1520-0477\(1999\)080%3c0245:tioscr%3e2.0.co;2](https://doi.org/10.1175/1520-0477(1999)080%3c0245:tioscr%3e2.0.co;2)
- Zhang C (2013) Madden-Julian oscillation: bridging weather and climate. *Bull Am Meteorol Soc* 94:1849–1870. <https://doi.org/10.1175/BAMS-D-12-00026.1>

Publisher's Note Springer Nature remains neutral with regard to jurisdictional claims in published maps and institutional affiliations.